JOURNAL OF AIRCRAFT
Vol. 37, No. 5, September–October 2000

Performance Enhancement of a Composite Tilt-Rotor Using Aeroelastic Tailoring

Ömer Soykasap* and Dewey H. Hodges†
Georgia Institute of Technology, Atlanta, Georgia 30332-0150

An optimization technique is applied in an attempt to improve the performance of a tilt-rotor aircraft with composite blades that are enhanced by aeroelastic tailoring. The aeroelastic analysis is based on a published mixed variational formulation of the exact intrinsic equations of motion of beams, along with a finite-state dynamic inflow theory for the rotor. The composite rotor blade is modeled structurally as a composite box beam with nonstructural mass included. For optimization the design variables are blade twist, box dimensions and wall thicknesses, ply angles of the laminated walls, and nonstructural mass. The rotor is optimized using an objective function that is weighted equally between the figure of merit in hover and the axial efficiency in forward flight. Constraints are considered on blade weight, autorotational inertia, geometry, and aeroelastic stability. The effects of all structural couplings on rotor performance are studied. Of all possible couplings, extension-twist coupling is found to be the most effective parameter to enhance performance. The effects of accounting for pretwist and thin- vs thick-walled theories in the blade cross-sectional analysis are discussed. Significant improvements in the objective function are shown to be possible even when optimizing only the extension-twist coupling of the rotor blade.

Introduction

DURING the past decades of rotorcraft development, many rotorcraft concepts have been suggested to achieve high-speed capability while maintaining good helicopter performance. Although many concepts have been considered as candidate aircraft, only the tilt-rotor aircraft remains a serious and practical configuration. Successful tilt-rotor designs in military applications, such as the XV-15 and the V-22 Osprey, fostered a civil version tilt-rotor, the Bell/Augusta 609, which is currently being developed.

Structural and aerodynamic parameters of a tilt-rotor represent a compromise design between helicopter and airplane modes. The well-known parameters in tilt-rotor design are twist distribution, mass distribution, and airfoil type of the rotor blades, along with rotor parameters including disc loading, downwash, and rotor angular speed. Some less-known parameters include structural couplings, such as extension-twist and bending-twist couplings. Early tilt-rotor studies were done by Alexander et al.[1] by optimizing the rotor-blade twist distribution for both flight modes. Lake et al.[2] pointed out the feasibility of passive blade twist control by varying the mass distribution along the blade.

Composite materials have been used in rotor-blade design because of their potential benefits. For example, the difference in rotor speeds between hover and forward flight modes causes a change in the blade centrifugal forces so that extension-twist structural coupling can be optimized for a given tilt-rotor.[3,4] Several researchers have focused on aeroelastic response of composite rotors to improve aircraft performance such as Chandra and Chopra,[5] Barwey and Peters,[6] Ganguli and Chopra.[7] Recently, Chattopadhyay et al.[8] developed a multilevel optimization procedure for high-speed prop-rotors using composite tailoring. More recently, Soykasap and Hodges[9] studied aeroelastic optimization of a composite tilt-rotor and demonstrated the feasibility of extension-twist coupling in the rotor blade. Not considered in earlier studies were effects of the other couplings such as bending-twist and extension-bending, the effect of pretwist on blade cross-sectional properties, or relaxation of the thin-walled modeling assumption.

By use of an integrated analysis, including three-dimensional aerodynamics and a finite element structural model for the blade, an attempt has been made to improve composite tilt-rotor performance using aeroelastic tailoring in the present study. The rotor aeroelastic analysis is performed by using a mixed variational formulation based on the exact intrinsic equations of motion for beams attached to moving frames[10] and the finite-state dynamic inflow theory by Peters and He.[11] Tilt-rotor performance is enhanced by optimizing the figure of merit in hover and the axial efficiency in forward flight. Building on previous work, Ref. 9 is extended to include effects of other structural couplings. Furthermore, isolated rotor stability is investigated, the influence of initial twist is included in the calculation of blade stiffness coefficients, and the effect of rotor speed on the performance is studied.

Structural Analysis

The rotor has three identical composite blades, each modeled as a laminated composite box beam inside an airfoil-shaped cavity with nonstructural mass. Schematics of a blade cross section and of a rotor blade are shown in Figs. 1 and 2, respectively. The analysis consists of an integrated set of programs, which perform a two-dimensional cross-sectional analysis of the rotor blade, followed by a one-dimensional aeroelastic finite element analysis of an isolated rotor. (The aeromechanical stability of the wing-rotor system is analyzed by use of a separate specialized package described next.)

Two-Dimensional Cross-Sectional Analysis

Prior to the execution of the isolated rotor analysis, cross-sectional properties must be determined. In the cross-sectional analysis there are two approaches discussed. One is restricted to a thin-walled beam and gives closed-form expressions for all of the stiffnesses. Beam-stiffness coefficients are obtained by using an anisotropic, thin-walled, closed-section beam theory by Berdichevsky et al.[12] During the derivation of the expressions, some parameters are neglected, such as pretwist and curvature effects. (Pretwist and initial curvature effects in the cross-sectional analysis are less significant than those in the one-dimensional equations, but these effects are not negligible in either place, in general.[13]) When the analytical cross-sectional analysis is applicable, it yields substantial time savings, calculating the stiffnesses within a small percentage error. However,

Presented as Paper 99-1475 at the AIAA/ASME/ASCE/ASC 40th Structures, Structural Dynamics, and Materials Conference, St. Louis, MO, 12–15 April 1999; received 20 July 1999; revision received 5 February 2000; accepted for publication 22 March 2000.

*Graduate Research Assistant, School of Aerospace Engineering; currently Assistant Professor, Faculty of Technical Education, Afyon Kocatepe University, Izmiryolu 7. km, Afyon, 03200, Turkey. Student Member AIAA.
†Professor, School of Aerospace Engineering. Fellow AIAA.

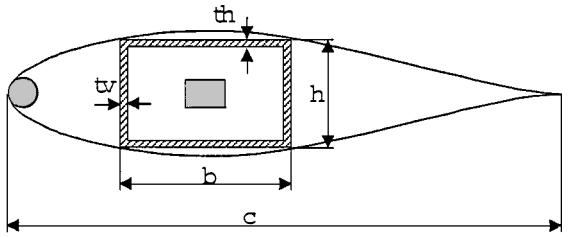

Fig. 1 Blade cross section.

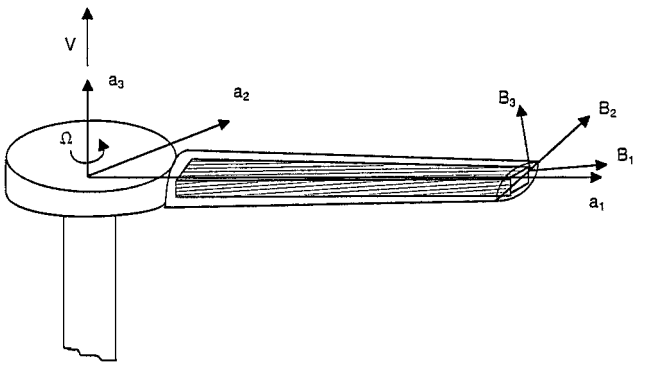

Fig. 2 Spanwise blade details.

the analytical approach can yield significant errors if its limitations are violated.[14] The other type of approach, a numerical one, is embodied in the variational asymptotic beam section (VABS) code.[15] VABS calculates the cross-sectional properties by the use of the finite element method. Thus, it can model any kind of cross section and is not restricted to thin-walled beams. The main drawback of using VABS in optimization is that the function evaluations become very expensive.

One-Dimensional Finite Element Analysis

The structural analysis uses the nonlinear beam theory of Hodges.[10] The theory is based on the exact intrinsic equations of motion for initially curved and twisted beams in a moving frame. The intrinsic equations of motion are derived from the extended form of Hamilton's principle as

$$\int_{t_1}^{t_2}\int_0^R [\delta(K-U)+\overline{\delta W}]\,\mathrm{d}r\,\mathrm{d}t = \overline{\delta A} \tag{1}$$

where K and U are kinetic and strain energy densities per unit length, respectively; $\overline{\delta A}$ is the virtual action at the ends of the beam and at the ends of the time interval $t_1 \le t \le t_2$; $\overline{\delta W}$ is the virtual work of the aerodynamic loads per unit length; and r is the rotor radial coordinate, with maximum value R. The bars over $\overline{\delta A}$ and $\overline{\delta W}$ indicate that they need not be variations of functionals.

The internal force and moment column matrices F_B and M_B and linear and angular momentum column matrices P_B and H_B are introduced by requiring

$$F_B = \left(\frac{\partial U}{\partial \gamma}\right)^T, \qquad M_B = \left(\frac{\partial U}{\partial \kappa}\right)^T$$

$$P_B = \left(\frac{\partial K}{\partial V_B}\right)^T, \qquad H_B = \left(\frac{\partial K}{\partial \Omega_B}\right)^T \tag{2}$$

where the subscript B denotes the deformed blade cross-sectional reference frame, and γ and κ are the force and moment strains measures, respectively. Similarly, V_B and Ω_B are the measures of reference line velocity and cross-sectional frame angular velocity in the deformed beam coordinate system, respectively.

The beam constitutive laws relate the strain and force measures and velocity and momentum measures as

$$\begin{Bmatrix} F_B \\ M_B \end{Bmatrix} = [S]\begin{Bmatrix} \gamma \\ \kappa \end{Bmatrix}, \qquad \begin{Bmatrix} P_B \\ H_B \end{Bmatrix} = \begin{bmatrix} m\Delta & -m_e \\ m_e & I \end{bmatrix}\begin{Bmatrix} V_B \\ \Omega_B \end{Bmatrix} \tag{3}$$

where S is the matrix of cross-sectional stiffness coefficients; m is the mass per unit length of the beam; Δ is a 3×3 identity matrix; m_e is a nonzero, antisymmetric containing the offsets between the beam reference line and the cross-sectional mass centroid; and I is the matrix of cross-sectional mass moments of inertia.

The variational formulation is given by

$$\int_{t_1}^{t_2}\int_0^R \left(\delta V_B^{*T} P_B + \delta\Omega_B^{*T} H_B - \delta\gamma^{*T} F_B - \delta\kappa^{*T} M_B + \overline{\delta W}\right)\mathrm{d}r\,\mathrm{d}t = \overline{\delta A} \tag{4}$$

where $(\,)^*$ denotes the geometrically exact expressions for velocity, angular velocity, force strain, and moment strain, given by

$$V_B^* = C^{Ba}(v_a + \dot{u}_a + \tilde{\omega}_a u_a)$$

$$\Omega_B^* = C^{ba}\left(\frac{\Delta - \tilde{\theta}/2}{1+\theta^T\theta/4}\right)\dot{\theta} + C^{Ba}\omega_a$$

$$\gamma^* = C^{Ba}\left(C^{ab}e_1 + u_a'\right) - e_1, \qquad \kappa^* = C^{ba}\left(\frac{\Delta - \tilde{\theta}/2}{1+\theta^T\theta/4}\right)\theta' \tag{5}$$

The subscripts and superscripts a, b, and B denote the rotating rotor frame, the undeformed blade cross-sectional reference frame, and the deformed blade cross-sectional reference frame, respectively. C^{ba} is the transformation matrix from frame a to frame b; u_a is the column matrix of displacement measures in the a frame; θ is the column matrix defined as $\theta_i = 2\beta_i \tan(\alpha/2)$ with the angle of rotation α about the unit vector $[\beta_1, \beta_2, \beta_3]^T$. Here e_1 is $[1, 0, 0]^T$; v_a is the column matrix of inertial velocity measures of the undeformed beam reference line in the a frame; ω_a is the column matrix of inertial rotor angular velocity measures in the a frame; $\tilde{(\,)}$ denotes the 3×3 antisymmetric cross-product operator matrix associated with the 3×1 column matrix $(\,)$; $\dot{(\,)}$ is the partial derivative with respect to t; and $(\,)'$ is the partial derivative with respect to the beam axial coordinate x_1.

Lagrange multipliers are used so that V_B, ω_B, γ, and κ satisfy the geometric relations in Eq. (5). After some algebraic manipulation one can express all of the governing equations in the weakest possible form to obtain

$$\int_{t_1}^{t_2} \delta\Pi_a\,\mathrm{d}t = 0 \tag{6}$$

where, for a beam of length l, we have

$$\begin{aligned}\delta\Pi_a = \int_0^l \Big\{ & \delta u_a'^T C^T C^{ab} F_B + \delta u_a^T\left[\left(C^T C^{ab} P_B\right)^{\cdot} + \tilde{\omega}_a C^T C^{ab} P_B\right] \\ & + \overline{\delta\psi_a'}^T C^T C^{ab} M_B - \overline{\delta\psi}_a^T C^T C^{ab}(\tilde{e}_1 + \tilde{\gamma})F_B \\ & + \overline{\delta\psi}_a^T\left[\left(C^T C^{ab} H_B\right)^{\cdot} + \tilde{\omega}_a C^T C^{ab} H_B + C^T C^{ab}\tilde{V}_B P_B\right] \\ & - \overline{\delta F}_a^T\left[C^T C^{ab}(e_1+\gamma) - C^{ab}e_1\right] - \overline{\delta F}_a'^T u_a \\ & - \overline{\delta M}_a^T\left(\Delta + \frac{\tilde{\theta}}{2} + \frac{\theta\theta^T}{4}\right)C^{ab}\kappa - \overline{\delta M}'^T\theta \\ & + \overline{\delta P}_a^T\left(C^T C^{ab} V_B - v_a - \tilde{\omega}_a u_a\right) - \overline{\delta P}_a^T\dot{u}_a \\ & + \overline{\delta H}_a^T\left(\Delta - \frac{\tilde{\theta}}{2} + \frac{\theta\theta^T}{4}\right)\left(C^T C^{ab}\Omega_B - \omega_a\right) \\ & - \overline{\delta H}_a^T\dot{\theta} - \delta u_a^T f_a - \overline{\delta\psi}_a^T m_a\Big\}\,\mathrm{d}x_1 \\ & - \left(\delta u_a^T\hat{F}_a + \overline{\delta\psi}_a^T\hat{M}_a - \overline{\delta F}_a^T\hat{u}_a - \overline{\delta M}_a^T\hat{\theta}\right)\Big|_0^l \end{aligned} \tag{7}$$

In Eq. (7) f_a and m_a are column matrices of measure numbers in a of the external force and moment vectors, respectively, which come from aerodynamic loads. The $\hat{(\ )}$ terms are the boundary values of the corresponding quantities.

To divide the blade into N finite elements, Eq. (6) can be written as

$$\int_{t_1}^{t_2} \sum_{i=1}^{N} \delta\Pi_i \, \mathrm{d}t = 0 \tag{8}$$

The following transformation and interpolation are applied within each element:

$$x = x_i + \xi \Delta l_i, \qquad \mathrm{d}x = \Delta l_i \, \mathrm{d}\xi, \qquad ()' = \frac{1}{\Delta l_i}\frac{\mathrm{d}}{\mathrm{d}\xi}()$$

$$\delta u_a = \delta u_i(1-\xi) + \delta u_{i+1}\xi, \qquad u_a = u_i$$

$$\overline{\delta\psi}_a = \overline{\delta\psi}_i(1-\xi) + \overline{\delta\psi}_{i+1}\xi, \qquad \theta = \theta_i$$

$$\overline{\delta F}_a = \overline{\delta F}_i(1-\xi) + \overline{\delta F}_{i+1}\xi, \qquad F_B = F_i$$

$$\overline{\delta M}_a = \overline{\delta M}_i(1-\xi) + \overline{\delta M}_{i+1}\xi, \qquad M_B = M_i$$

$$\overline{\delta P}_a = \overline{\delta P}_i, \qquad P_B = P_i, \qquad \overline{\delta H}_a = \overline{\delta H}_i, \qquad H_B = H_i \tag{9}$$

where u_i, θ_i, F_i, M_i, P_i, and H_i are constant within each element; all δ quantities are arbitrary; and ξ varies from 0 to 1.

The final structural equations can be written in the rotating frame as

$$F_S(X, \dot{X}) - F_L(X, Y, \dot{X}) = 0 \tag{10}$$

where $F_S(\ )$ and $F_L(\ )$ are the structural and lift operators, respectively; X is the column matrix of unknown structural variables

$$X = \left[\hat{F}_1^T \quad \hat{M}_1^T \quad u_1^T \quad \theta_1^T \quad F_1^T \quad M_1^T \quad P_1^T \quad H_1^T \quad \cdots \quad u_N^T \quad \theta_N^T \quad F_N^T \quad M_N^T \quad P_N^T \quad H_N^T \quad \hat{u}_{N+1}^T \quad \hat{\theta}_{N+1}^T\right]^T \tag{11}$$

and Y is the column matrix of unknown inflow state variables, given in the aerodynamic analysis.

Aerodynamic Analysis

Lift Model

For a thin airfoil the aerodynamic loads consist of both circulatory and noncirculatory forces and moments as in Ref. 16:

$$f_{B_2} = \frac{1}{2}\rho_\infty c a\left[\left(W_{B_3} - \frac{c}{2}\Omega_1\right)W_{B_3} - \frac{c_d}{a}W_{B_2}W\right]$$

$$f_{B_3} = \frac{1}{2}\rho_\infty c a\left[\left(\frac{c}{2}\Omega_1 - W_{B_3}\right)W_{B_2} - \frac{c_d}{a}W_{B_3}W - \frac{c}{4}\dot{V}_{B_3} + \frac{c^2}{16}\dot{\Omega}_1\right]$$

$$m_{B_1} = -\frac{1}{32}\rho_\infty c^3 a\left(W_{B_2}\Omega_1 - \dot{V}_{B_3} + \frac{3c}{8}\dot{\Omega}_1\right)$$

$$f_{B_1} = m_{B_2} = m_{B_3} = 0 \tag{12}$$

where Ω_1 is the component of blade angular velocity along the $\boldsymbol{B}_1$ direction; ρ_∞, c, a, and c_d are the mass density of the air, the chord length, the lift curve slope, and the drag coefficient, respectively; and W is the relative wind speed with W_{B_2} and W_{B_3} being the relative wind measures in the B frame, given by

$$W_{B_2} = e_2^T C^{ba} C(v_a + \tilde{\omega}_a u_a + \dot{u}_a + \lambda e_3)$$

$$W_{B_3} = e_3^T C^{ba} C(v_a + \tilde{\omega}_a u_a + \dot{u}_a + \lambda e_3) \tag{13}$$

where λ is the induced inflow velocity.

Inflow Model

The inflow model uses the finite-state dynamic inflow theory by Peters and He.[11] In this theory the blade sectional aerodynamic lift, drag, and moment are based on thin-airfoil theory, whereas the unsteady induced inflow velocity is computed from a three-dimensional generalized dynamic wake theory. The resultant airloads are both three-dimensional and unsteady. The dynamic wake theory is developed from incompressible potential flow. The unsteady induced flow is related to the blade aerodynamic lift by a system of first-order ordinary differential equations written in the rotating frame as

$$\begin{bmatrix} [K_n^m] & 0 \\ 0 & [K_n^m] \end{bmatrix} \begin{Bmatrix} \{a_n^m\} \\ \{b_n^m\} \end{Bmatrix}^* + \begin{bmatrix} [B_{nt}^m][V_n^m] & -m[K_n^m] \\ m[K_n^m] & [B_{nt}^m][V_n^m] \end{bmatrix} \begin{Bmatrix} \{a_t^m\} \\ \{b_t^m\} \end{Bmatrix} = \frac{1}{2}\begin{Bmatrix} \{\hat{\tau}_n^m\}^c \\ \{\hat{\tau}_n^m\}^s \end{Bmatrix} \tag{14}$$

where a_n^m and b_n^m are the modal inflow states. The $\hat{\tau}_n^m$ are the generalized inflow forcing functions and are obtained by spanwise integration of blade aerodynamic lift. The $(\ )^*$ implies a nondimensional time derivative. The inflow is expanded as

$$\bar{\lambda}(\bar{r}, \bar{\psi}, \bar{t}) = \sum_{m=0}^{\infty} \sum_{n=m+1,m+3,\ldots}^{\infty} \phi_n^m(\bar{r})\left[a_n^m(\bar{t})\cos(m\hat{\psi}) + b_n^m(\bar{t})\sin(m\hat{\psi})\right] \tag{15}$$

where $\bar{r}$ is the nondimensional radial coordinate, $\hat{\psi}$ is the azimuth coordinate, $\bar{t}$ is the nondimensional time Ωt, and the $\phi_n^m(\bar{r})$ are the radial inflow shape functions.

The inflow state variables and inflow equations can be written as

$$Y = \left[\cdots \left\{a_n^m\right\}^T \cdots \cdots \left\{b_n^m\right\}^T \cdots\right]^T \tag{16}$$

$$-F_P(X, Y) + F_I(Y, \dot{Y}) = 0 \tag{17}$$

where $F_P(X, Y)$ and $F_I(Y, \dot{Y})$ are the pressure and inflow operators and represent the right-hand side and left-hand sides of Eq. (14), respectively.

Aeroelastic Analysis

The governing system equations can now be written in the form

$$F_S(X, \dot{X}) - F_L(X, Y, \dot{X}) = 0$$

$$-F_P(X, Y) + F_I(Y, \dot{Y}) = 0 \tag{18}$$

The problem can be considered in two parts: steady-state (independent of time) and transient (time-dependent) responses. The unknown variables are taken to be

$$\begin{Bmatrix} X \\ Y \end{Bmatrix} = \begin{Bmatrix} \bar{X} \\ \bar{Y} \end{Bmatrix} + \begin{Bmatrix} \check{X}(t) \\ \check{Y}(t) \end{Bmatrix} \tag{19}$$

where $\bar{X}$, $\bar{Y}$ are the steady components and $\check{X}(t)$, $\check{Y}(t)$ are the transient components of the solution.

Steady-State Response

In the case of the steady-state response, all blades are deformed the same amount for all time. The system equations thus reduce to

$$F_S(\bar{X}) - F_L(\bar{X}, \bar{Y}) = 0, \qquad -F_P(\bar{X}, \bar{Y}) + F_I(\bar{Y}) = 0 \quad (20)$$

The steady-state rotor aeroelastic response is obtained for a given operating state, either in hover or axial flight. A trim procedure is added to the system to get desired values of thrust, in which an iterative scheme for the controls is considered. The control variables include collective pitch and cyclic pitch. Cyclic pitch is ignored in the study for the sake of simplicity because the effect of it is quite small for steady-state response.[17]

The steady-state response is obtained by using the computer code AEROSCOR (Aeroelastic Stability of Composite Rotors), written by Shang and based on Ref. 16, extended for this study to include axial flow and cyclic modes. In the steady-state analysis the nonlinear structural and inflow equations are solved iteratively by the Newton–Raphson method.

In a gimballed rotor, blades are attached to the hub without flap or lag hinges, and the hub itself is connected to the rotor shaft by a universal joint or gimbal. As explained in Ref. 18, during the coning motion each blade behaves as cantilevered, generating no net pitch or roll moment on the rotor. Thus, in this study the steady-state solution is obtained by assuming cantilever boundary conditions.

Isolated Rotor Stability

Aeroelastic stability of the system is investigated by calculation of the eigenvalues of the resulting linear, constant-coefficient, ordinary differential equations obtained by perturbation of the steady state. For isolated rotor stability the cantilever boundary conditions are assumed for the collective mode, whereas pinned-free boundary conditions for flapping only are applied to the cyclic modes.

The blade equations are written in the rotating frame, representing the motion of an individual rotor blade. The inflow equations are written in the rotating frame, yet representing the inflow of the rotor. Therefore a special multiblade coordinate transformation is needed to represent the rotor behavior—one in the rotating frame. The transformation is carried out to generate three sets of equations for collective, differential, and cyclic modes as follows:

$$\check{X}_q = \check{X}_0 + (-1)^q \check{X}_d + \check{X}_c \cos(\hat{\psi}_q) + \check{X}_s \sin(\hat{\psi}_q) \quad (21)$$

where q is the index of the blade, X_0 and X_d are collective and differential modes, respectively, and X_c and X_s are cyclic modes. The differential mode only exists when the rotor has an even number of blades. Inflow variables are separated for collective, differential, and cyclic modes as

$$\check{Y} = \check{Y}_0 + \check{Y}_d + \check{Y}_c \quad (22)$$

The final stability equations of a perturbed system are written for collective, differential, and cyclic modes as follows:

$$[A]\begin{Bmatrix} \dot{\check{X}} \\ \dot{\check{Y}} \end{Bmatrix} + [B]\begin{Bmatrix} \check{X} \\ \check{Y} \end{Bmatrix} = \begin{Bmatrix} 0 \\ 0 \end{Bmatrix} \quad (23)$$

Whirl Stability

A whirl stability analysis is needed in order not to limit the forward speed of the tilt-rotor aircraft. Because the aeromechanical stability of a tilt-rotor is most significantly affected by the wing stiffness and the blade mass distribution, we choose to investigate it here by using the available computer program RAPID (Rotorcraft Analysis for Preliminary Design).[19] RAPID solves for the nonlinear system trim response and performs an eigenvalue analysis about the nonlinear trim solution. Because RAPID assumes a rigid blade, the optimization only affects the blade mass and twist distribution. Because these calculations take a few hours on a Pentium II class computer (133 MHz), RAPID is really not rapid relative to the steady-state response and isolated rotor stability calculations. To avoid slowing down the optimization, then, the stability is only checked at the end of the optimization. However, the whirl stability analysis would have to be implemented within the optimization if the optimized configuration were to exhibit a whirl instability. Fortunately, for this study it does not.

Optimization Problem

The optimization problem is posed as a constrained maximization problem with a multiobjective function. During the optimization, the figure of merit in hover and the axial efficiency in forward flight are maximized simultaneously for specified flight conditions. In hover, the figure of merit is $F_M = C_T^{3/2}/[\sqrt{(2)}C_P]$. In forward flight the axial efficiency is defined as $\eta_{cr} = TV/P$. Weighting factors are imposed to reduce this multiobjective problem to a single objective problem.

The figure of merit F_M is a comparison of the actual rotor performance with that of the ideal rotor. To improve the hover performance, the rotor power must be minimum for a given operating condition. In hover the total power consists of induced power and profile power. The former is necessary to produce the thrust, and the latter is inevitably lost owing to the drag of the blades. However, the loss can be reduced by using advanced airfoils. Momentum theory suggests that the inflow distribution over the blade must be uniform for an ideal rotor.

In forward flight the rotor power consists of induced power (includes the axial power) and profile power. The total inflow over the rotor disk increases because of axial speed, causing a decrease in induced inflow velocity. The sectional angle of attack of the rotor blades depends on pitch and inflow angles:

$$\alpha(r) = \theta(r) - \phi(r), \qquad \theta(r) = \theta_0 + \theta_t(r) + \theta_e(r) \quad (24)$$

where θ_0 is the collective pitch angle, θ_t is the local built-in twist angle, and θ_e is the local angle of elastic twist. Most of the inflow angle $\phi(r)$ in forward flight comes from axial flow. For an angle of attack to be feasible, the pitch angle must be higher than the inflow angle.

The design variables for the optimization consist of both aerodynamic and structural parameters. The blade is discretized into 12 finite elements. The blade twist, box width and height, horizontal and vertical wall thicknesses, and nonstructural mass concentrated at the quarter-chord are allowed to be different in each finite element, whereas the ply angle for the laminated walls is assumed to be constant along the blade in order to provide extension-twist coupling and manufacturing ease. There are side constraints imposed on all design variables to ensure a meaningful design.

Constraints imposed on the optimization are blade weight, autorotational inertia, strength, geometry, and aeroelastic stability. The assumption is made that the number of blades, rotor radius, airfoil distribution, rotor angular speed, and chord distribution are constant during the optimization. The inequality constraints are as follows. First, the blade mass, which is the structural mass plus any nonstructural mass, is constrained, so as not to increase manufacturing cost. To use thin-walled box-beam theory, the ratio of wall thickness to the box major dimensions should be less than 10%; this is imposed as a constraint except as noted here. In case of power failure, the autorotational inertia of the blade must be greater than a specified reference value. To prevent blade stall, angles of attack for both flight regimes are constrained at the three-quarter radius. The blade is subject to aerodynamic loads (lift, drag, and pitching moment) as well as centrifugal loads. The structural variables for each finite elements of the blade are obtained by solving the system equations. After calculating maximum stresses in the cross section of the box-beam, a failure criterion is needed to prevent material failure. In this study the Tsai–Wu failure criterion is used to prevent the optimizer from selecting a structural configuration in which the blade root stresses are too large. Finally, to prevent isolated rotor instability in both flight regimes as well as the destabilization of the rotor/wing in forward flight, aeroelastic stability constraints are imposed. For a stable solution the real part of all eigenvalues must be less than zero.

The optimization problem may then be stated as follows. Maximize

$$F(X) = K_1 F_M + K_2 \eta_{cr}$$

$$g_i(X) \leq 0 \qquad \text{for} \qquad i = 1, \ldots, m$$

Subject to

$$h_j(X) = 0 \qquad \text{for} \qquad j = 1, 2$$

$$X_i^l \leq X_i \leq X_i^u \qquad \text{for} \qquad i = 1, \ldots, n \tag{25}$$

where K_1 and K_2 are the weighting factors chosen by the user. The equality constraints are

$$h_1 = T_{\text{hover}} - (T_{\text{hover}})_{\text{ref}} = 0, \qquad h_2 = T_{\text{cruise}} - (T_{\text{cruise}})_{\text{ref}} = 0 \tag{26}$$

At each optimization step the rotor is trimmed by adjusting the collective pitch angle θ_0 so that the equality constraints are satisfied.

The automated design synthesis optimization code[20] is used as the optimizer. A feasible direction technique is used for optimization. The gradients of the objective function and constraints are obtained numerically by using the forward finite difference approach.

Optimization Results

The reference rotor optimized has the same configuration parameters as those of an existing three-bladed gimballed rotor, an XV-15 with metal blades. The rotor properties are given in Table 1. The planform, thickness, and twist distribution of the rotor are given in Figs. 3 and 4.

Aeroelastic optimization is performed at typical operating points of $C_T/\sigma = 0.13$ and $\Omega = 565$ rpm at sea level for hover and $C_T/\sigma = 0.046, \Omega = 458$ rpm, and $V = 300$ knots at 25,000 ft for forward flight. The lift curve slope of the airfoil is corrected for compressibility effects as suggested by Ref. 18:

$$a = \frac{a_{\text{incomp}}}{\sqrt{1 - M^2}} \tag{27}$$

Table 1 Rotor properties

Parameter	Value
Number of blades Q	3
Radius of rotor disc R	3.81 m
Blade chord c	35.6 cm
Blade mass m_{ref}	47.48 kg
Precone angle β_0	2.5 deg
Autorotation inertia $I_{A_{\text{ref}}}$	109.89 kg-m^2
Coefficient of drag c_{D_0}	0.008
Lift curve slope a_{hover}	5.2

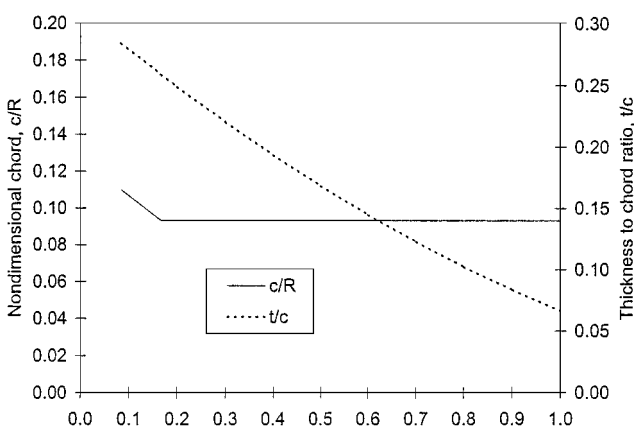

Fig. 3 Blade chord and thickness distribution.

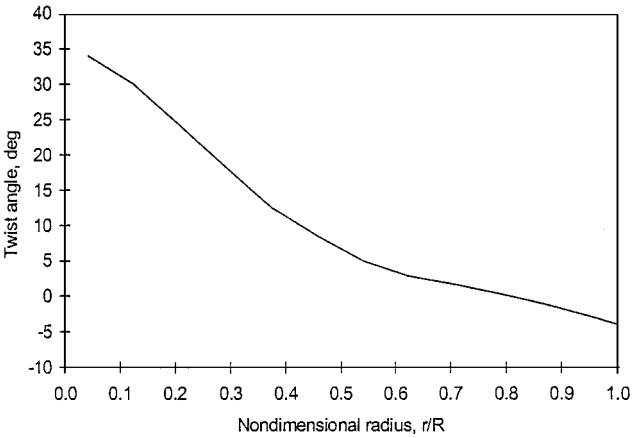

Fig. 4 Blade twist distribution.

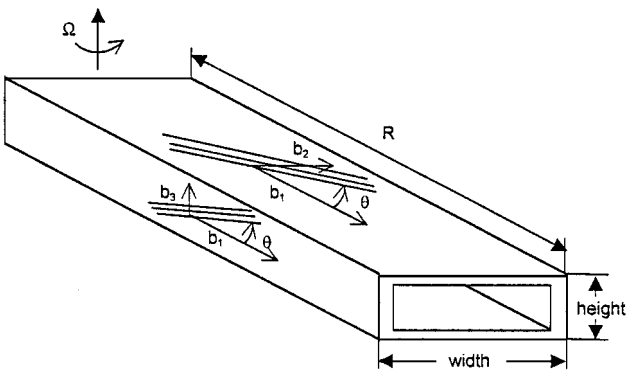

Fig. 5 Ply angle definition.

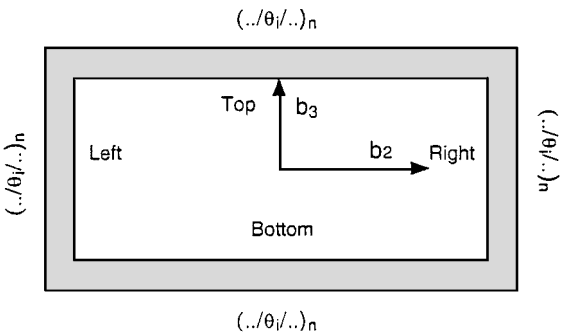

Fig. 6 Extension-twist coupled box beam.

The aircraft is capable of high duration hover (approximately 1 h at design gross weight), helicopter mode flight, and airplane mode level flight at speeds greater than 300 kn. The weighting factors are taken to be $K_1 = K_2 = 0.5$ for this aircraft. The flutter-free requirement of the XV-15 is $1.2V_D$ (360 kn at sea level).[21] The box beam is assumed to be made of AS4/3501-6 graphite/epoxy. The material properties are $E_1 = 1.42 \times 10^{11}$ N/m^2, $E_2 = E_3 = 9.8 \times 10^9$ N/m^2, $G_{12} = G_{13} = 6.0 \times 10^9$ N/m^2, $G_{23} = 4.83 \times 10^9$ N/m^2, $\rho = 1603$ kg/m^3, $\nu_{12} = \nu_{13} = 0.42$, and $\nu_{23} = 0.5$. Each wall used to model the box beam is made of laminated orthotropic composite plies.

Extension-Twist Coupled Box Beam

Extension-twist coupling is chosen as the variable with the most potential to optimize the rotor performance. For a given cross section extension-twist coupling can be created by wrapping the layups using the filament-winding technique. The ply angle is defined as the angle between the fiber direction and the spanwise unit vector $\boldsymbol{b}_1$, as shown in Fig. 5. Such a cross section has the same stacking sequence for each wall (see Fig. 6) and provides a so-called circumferentially uniform stiffness. A positive ply angle produces

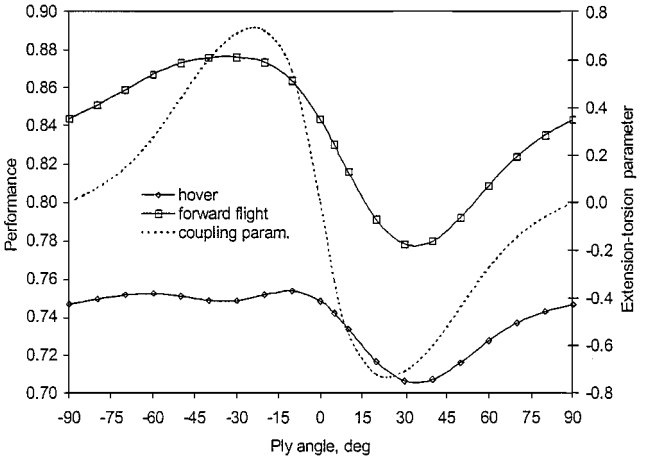

Fig. 7 Effect of ply angle on the performance.

negative extension-twist coupling and vice versa. Sometimes this configuration is also called an antisymmetric configuration because the layups are antisymmetric with respect to the cross-sectional midplanes. Moreover, use of a single-ply angle around the contour of the box beam is desirable to reduce hygrothermal deformation as studied numerically and experimentally by Lentz and Armanios.[22] Effects of other couplings are studied in the following section.

The optimum rotor blade is designed to maximize the performance in both flight regimes. To accomplish the multiobjective design goal, a multistep method is applied. First the results are obtained for the steady-state aeroelastic response and compared with the earlier test results. Then, the design sensitivities are investigated. Finally, an optimization strategy is chosen based on the sensitivity results. Steady-state results are validated with test results in Ref. 9.

The rotor response to the perturbations about the steady state is obtained for both hover and forward flight, and the effect of ply angle on the damping is investigated. For the collective modes in both flight regimes, the negative ply angle (positive extension-twist coupling) tends to increase the damping, particularly in hover. There is an unstable region in hover cyclic mode for ply angles greater than -5 deg. The results show that forward flight is free of instability. However, the accuracy of the present stability results remains to be validated due to the lack of experimental data.

The effect of the ply orientation angle and corresponding extension-twist parameter $\beta_{14} = S_{14}/\sqrt{(S_{11}S_{44})}$ on the rotor performance is shown in Fig. 7 for the case in which no constraints are imposed and other parameters including built-in twist distribution are kept constant. The performance in both flight regimes is very sensitive to the ply angle. As the extension-twist parameter changes with the ply angle, it affects the deformed twist distributions, changing the elastic twist distributions in both flight regimes. The twist change is based on the magnitudes of the coupling, axial force and torsional moment, and can be developed in desired directions in both flight regimes by varying the coupling for given loading conditions. In our case because the axial forces and torsional moments along the span of the rotor blade are different in hover and airplane modes, it is possible that some value of the coupling can be found so as to improve performance in both flight regimes.

For constrained optimization the results are obtained by first taking into account the ply angle as a design variable and angles of attack in hover and forward flight as constraints. Some extension-twist coupling, which yields a nose-up elastic twist, is needed for the baseline to make it have performance similar to that of the reference rotor. To this end, the ply angle is assumed to be 5 deg for the entire box beam of the baseline.

Optimum solutions are given in Table 2. The corresponding induced inflow velocities over the blade are given in Fig. 8 for hover and in Fig. 9 for forward flight. Elastic twist distributions for the optimized ply angles are given in Figs. 10 and 11. The elastic twists of the baseline are 2.8 deg for hover and 2.2 deg for forward flight, respectively. The optimal elastic twist in hover is -8 deg, whereas

Table 2 Optimum ply angle

Flight condition	Ply angle, deg	F_M	η_{cr}	Improvement, %
Baseline	5	0.7419	0.8213	—–
Hover	−10.83	0.7538	——	1.60
Forward flight	−34.10	——	0.8710	6.05
For both	−23.01	0.7505	0.8694	3.63

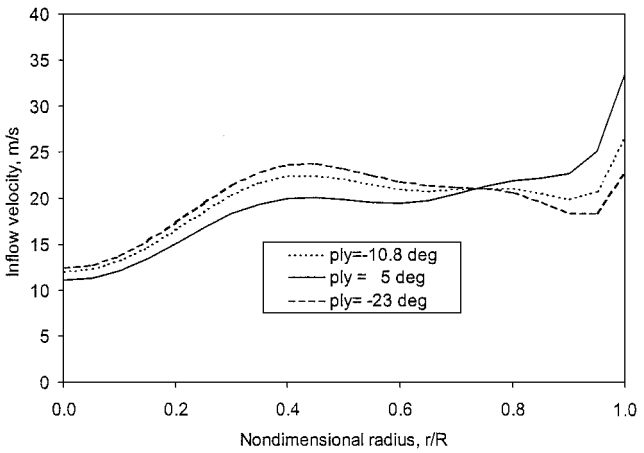

Fig. 8 Induced inflow distribution for optimized ply angles (hover).

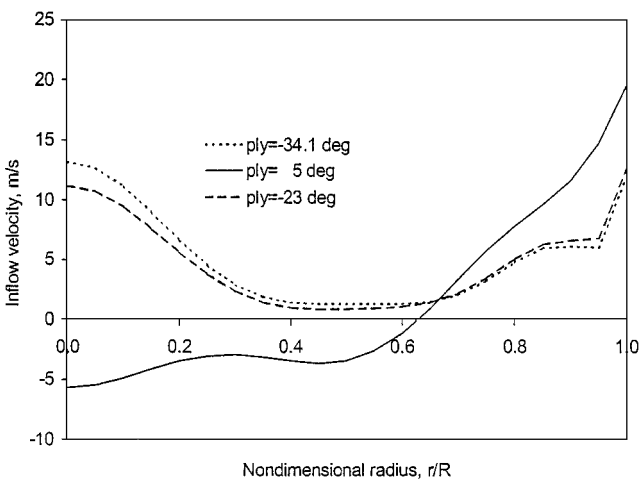

Fig. 9 Induced inflow distribution for optimized ply angles (forward flight).

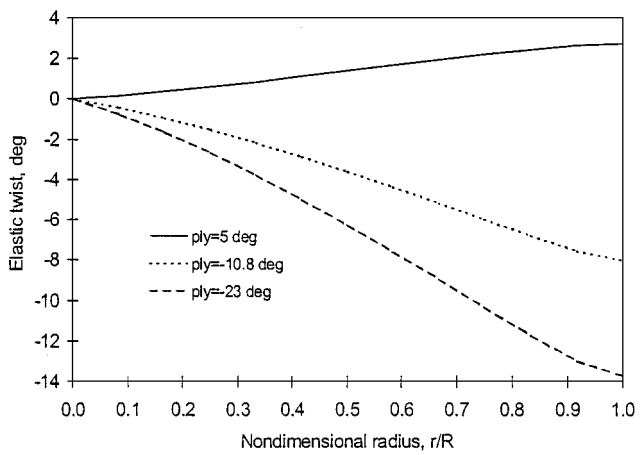

Fig. 10 Elastic twist distribution for optimized ply angles (hover).

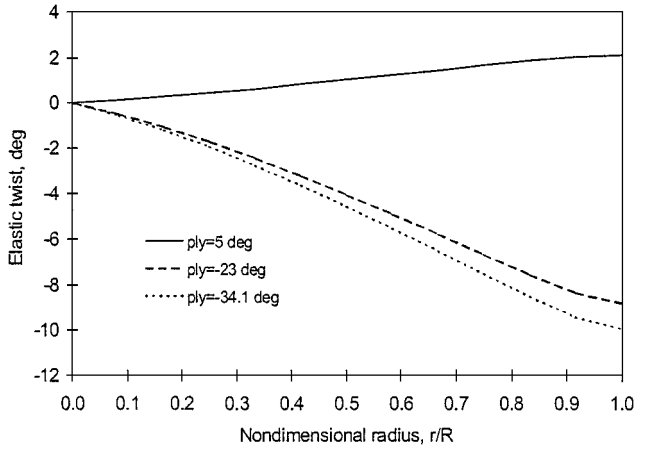

Fig. 11 Elastic twist distribution for optimized ply angles (forward flight).

the optimal elastic twist in forward flight is −9.9 deg. Optimizing the coupling in both flight regimes, one obtains elastic twists of −13.7 deg for hover and −8.8 deg for forward flight.

Next, the rotor angular speed is considered as a design parameter. The upper and lower limits of rotor angular speeds are restricted because of the drag divergence Mach number of the airfoils, the centrifugal force limits for the structural load path, and the maximum steady-state torque limit of the rotor shaft. The maximum steady-state torque of the reference rotor shaft is 130,000 lb-in. (14,688 Nm). Optimum angular speed in hover is obtained as 617.5 rpm ($F_M = 0.7462$) for the initial value of the ply angle. The rotor angular speed itself does play an important role in the performance. However, the effect of rotor speed on the hover performance is negligible (the improvement is less than 0.2%) after optimizing the ply angle. The optimum angular speed in forward flight is obtained as 414.6 rpm ($\eta_{cr} = 0.8426$) and 394.5 rpm ($\eta_{cr} = 0.8762$) for initial and optimal ply angles, respectively. Thus, decreasing the forward flight revolutions per minute would appear to be helpful. However, because of torque limitation, the effect of rotor speed on the forward flight performance is negligible (the improvement is 0.8% at the torque limit) after optimizing the ply angle. Therefore, the rotor angular speeds in both flight regimes will henceforth be assumed constant in the optimization.

The built-in twist at each section of the blade is considered as a design variable, along with the ply angle. Constraints are imposed on the local angles of attack. We choose two different starting points to investigate if there are local maxima: S1 refers to the baseline design, and S2 refers to the baseline design having optimum ply angle, −23 deg. The former yields $F_M = 0.7565$ and $\eta_{cr} = 0.8774$ with an improvement of 4.52%, whereas the latter yields $F_M = 0.7531$ and $\eta_{cr} = 0.8771$ with an improvement of 4.28%. The baseline blade has an initial twist of −33 deg over the productive part of the blade, from $r/R = 0.1$ to 1. The optimum solution (starting from S1) decreases the twist to −41.7 deg and decreases the ply angle to −0.7 deg, whereas optimum solution (starting from S2) decreases the twist to −33.8 deg, and decreases ply angle to −13 deg. This apparent discrepancy is a result of the fact that both the extension-twist coupling, and the built-in twist can be used to improve the performance so that both influence the deformed twist distribution. The optimization process results in two different configurations, representing local maxima. Starting with S1 yields more built-in twisted and less coupled blade than that with S2. Because the difference between local maxima is very small, this suggests that highly twisted and structurally uncoupled blades can be replaced by structurally coupled blades with less built-in twist if one starts with S2.

Then, the box-beam design variables and nonstructural masses as well as ply angle and twist are included in the optimization, which requires a total of 73 design variables. Angles of attack, blade mass, autorotation inertia, material failure, and aeroelastic stability are imposed as constraints. Following the result of the preceding optimization step, the S2 design is chosen as a starting point for the optimization to take advantage of extension-twist coupling. Starting from S2, the objective function is maximized. Compared to the initial values, the final design represents a 4.34% improvement in the objective function, yielding $F_M = 0.7553$ and $\eta_{cr} = 0.8756$. The final optimal solution increases the twist to −33.5 deg and decreases ply angle to −22.1 deg. The final design is able to improve the performance characteristics from the initial design and satisfies all constraints.

Bending-Twist Coupled Box Beam

Bending-twist coupling is created by layups which provide so-called circumferentially antisymmetric stiffness. In this case horizontal walls having θ_i layup on one side and $-\theta_i$ on the other side with respect to cross-section midplane produce flap-twist coupling (as shown in Fig. 12). Similarly, vertical walls having θ_i layup on one side and $-\theta_i$ on the other side with respect to the cross-sectional midplane produce lead-lag-twist coupling.

Balanced layups, represented by $[\cdots/(\zeta_i/-\zeta_i)\cdots/]_n$, are assumed to be made of zero-deg ply angle for the sake of simplicity because the major part of the coupling comes from antisymmetric layups for other walls. The results are obtained using a single design parameter θ, with angles of attack in hover and forward flight as constraints. Starting from $\theta = -5$ deg, optimum solutions are given in Tables 3 and 4 for a flap-twist coupled and a lead-lag-twist coupled box-beam, respectively. Results show that bending-twist coupling improves rotor performance, but the improvement is less than that of extension-twist coupling as found in Ref. 23.

Other Couplings

Extension-bending couplings can be created by using balanced layups, but in a different way for horizontal and vertical walls. Different balanced layups in horizontal walls produce extension-flap coupling, whereas different balanced layups in vertical walls produce extension-lead-lag coupling. Although the same balanced layups in either vertical or horizontal walls do not play an important role in the coupling, they affect the torsional rigidity. Therefore they need to be fixed during the optimization to see only the effect of the coupling. The same balanced layups are assumed to be made of zero-deg ply angle providing high torsional flexibility. The results with

Table 3 Optimum ply angle for flap-twistcoupled box beam

Flight condition	Ply angle, deg	F_M	η_{cr}	Improvement, %
Hover	−11.41	0.7524	——	1.42
Forward flight	−15.51	——	0.8531	3.87
For both	−14.63	0.7523	0.8530	2.70

Table 4 Optimum ply angle for lead-lag-twistcoupled box beam

Flight condition	Ply angle, deg	F_M	η_{cr}	Improvement, %
Hover	−2.55	0.7484	——	0.88
Forward flight	17.15	——	0.8382	2.06
For both	16.19	0.7481	0.8381	1.47

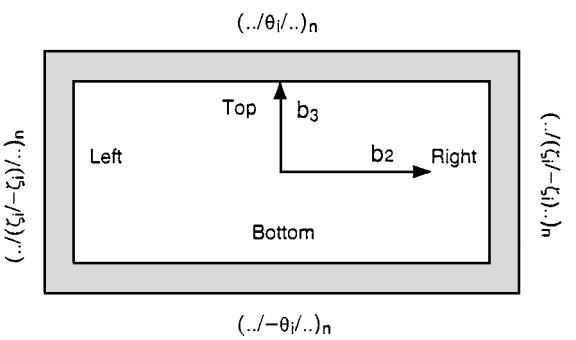

Fig. 12 Flap-twist coupled box beam.

the constraints of angles of attack in hover and forward flight show that extension-flap and extension-lead-lag couplings improve rotor performance by 1.4 and 1.3%, respectively, which are significantly less than the improvement attainable by use of extension-twist coupling. Moreover imposing other constraints including strength and stability would decrease the improvement attainable.

Extension-twist-bending couplings can be created by using the same balanced layups for either horizontal or vertical walls and different angle-ply layups for the rest. If there are no symmetric or antisymmetric layups with respect to cross-section midplane, a fully-coupled box beam is obtained. Extension-twist-bending and fully coupled box beams are also studied. The results are obtained by imposing angles of attack in hover and forward flight as constraints. The former improves the performance by 2.7%, whereas the latter improves by 3.6%. The improvement by fully coupled box beam is almost the same as using only extension-twist coupling. Thus, the use of more complicated layups does not really buy any performance enhancement and makes the manufacturing process more involved.

Optimization with VABS

Because of limitations in the applicability of the thin-walled approach, VABS may be used to get accurate results for the cross-sectional stiffnesses. However, such calculations take a lot of computer time (roughly 2 min on an HP 9000-735 computer for each cross section). VABS uses six-noded finite element meshes for the cross section. To speed up the optimization, two levels of optimization were considered. At the first level the results are obtained by the use of a crude mesh. After the optimization proceeds for a while, the mesh is refined, and the optimization is continued. In the crude mesh the cross section of the box is divided into a total of eight elements (2×1 for each wall), yielding errors in stiffnesses up to 5%, yet taking only 3.3 s per cross section. The refined mesh uses 96 elements (4×6 for each wall), keeping the errors less than 1%, yet taking 85 s.

Following the steps just mentioned, we obtained optimum ply angles for an extension-twist coupled box beam, which are given in Table 5. Obtaining stiffnesses from VABS, one finds a 0.4% increase in the performance with respect to thin-wall approach. In other words, the thin-walled approach results in an optimum configuration with an estimated performance that is 0.4% too low. Results that include the built-in twist as a design parameter are given in Tables 6 and 7, without and with the pretwist effect on the stiffnesses, respectively. (VABS uses the opposite sign convention for ply angles. The results presented are based on the sign convention of Fig. 5.) Inclusion of the pretwist angle in the stiffness calculations yields an average of 0.3% increase in the overall performance. As compared to the thin-walled approach, VABS gives a 1.3% improvement. This suggests that one can, for optimization purposes, improve the utility of closed-form expressions for the cross-sectional stiffnesses of thin-walled beams by modifying them so that pretwist is taken into account.

Table 5 Optimum ply angle using VABS

Flight condition	Ply angle, deg	F_M	η_{cr}	Improvement, %
Baseline	5.0	0.7419	0.8213	——
Hover	−12.18	0.7547	——	1.73
Forward flight	−33.88	——	0.8791	7.04
For both	−32.28	0.7510	0.8791	4.28

Table 6 Optimum ply angle and twist using VABS (without pretwist effect)

Optimization method	Ply angle, deg	Twist, deg	F_M	η_{cr}	Improvement, %
Opt. (S1)	−10.9	−46.9	0.7542	0.8916	5.28
Opt. (S2)	−15.0	−45.2	0.7549	0.8891	5.17

Table 7 Optimum ply angle and twist using VABS (with pretwist effect)

Optimization method	Ply angle, deg	Twist, deg	F_M	η_{cr}	Improvement, %
Opt. (S1)	−7.5	−50.5	0.7556	0.8938	5.51
Opt. (S2)	−6.1	−51.7	0.7558	0.8942	5.55

Conclusion

An optimization study on the performance of tilt-rotor aircraft has been presented. The present study shows that the built-in twist distribution and extension-twist structural coupling are key parameters affecting tilt-rotor performance when the airfoil distribution, rotor speed, and rotor radius are kept constant. Although rotor angular speed plays an important role in rotor performance, the effect of changing the rotor angular speed is negligible once ply angle and/or twist distribution are optimized.

As far as structural couplings are concerned, the most important coupling is found to be extension-twist coupling. Moreover, a blade with such coupling can be manufactured easily by the filament winding technique. A single-ply angle along the blade span and through the thickness of the box beam can be used. Such a configuration also offers a hygrothermally stable solution. The present research has shown that substantial improvements are not obtained by varying the ply angle (or extension-twist coupling) along the blade span as well as through the thickness. Highly twisted and structurally uncoupled rotor blades can be replaced by structurally coupled blades with less built-in twist. In spite of the simplicity of this configuration, the Tsai–Wu failure criterion does not predict material failure for the optimum blade design.

Structural couplings can be tailored for a tilt-rotor performance as long as failure criteria and stability boundaries are not violated. In this study isolated rotor stability is investigated for both hover and forward flight as well as whirl flutter. Although the isolated rotor instabilities are observed in hover when varying the ply angle to produce the extension-twist coupling, the optimized configuration is free of instability. However, the present stability results have not been validated because of a lack of published results (either analytical or experimental) for this type of configuration.

There were some questions raised by the earlier work of Nixon[23] about the possibility of achieving high extension-twist coupling and whirl-flutter instability stemming from the coupling. Previous work showed that the amount of the twist deformation caused by the coupling could be further increased by additional tip mass, but that adding the tip mass is found to be detrimental to whirl flutter. In the present work the couplings are obtained by the choice of layup of box beam without the addition of a tip mass. Whirl flutter is checked by RAPID for the final optimum solution.

Although our optimized configurations are shown to be free of whirl-flutter instability, one could argue that a more powerful tool than RAPID may need to be used. However, it appears to the authors that even if there were a negative effect of blade structural coupling on whirl flutter it could be alleviated by appropriately tailoring the wing stiffness, as suggested by recent studies.[24]

Another area in which the present work needs to be improved is the area of avoiding resonance conditions. The optimized configuration does have some frequencies near integer multiples of the rotor speed (see Ref. 14, pp. 85–87). Although this does not necessarily indicate there will be a problem, the underlying analysis for the optimization should be generalized to the point that such conditions can be rigorously examined. Moreover, the optimization should be reworked so as to avoid certain frequency ranges where appropriate.

At this stage it appears that enhancement of the rotor performance by optimizing twist (built-in twist as well as elastic twist) is both possible and practical. Thus, the capability of significantly enhancing rotor performance by use of structural coupling should not be ignored.

Acknowledgments

This work was supported through the Center of Excellence for Rotorcraft Technology, at Georgia Institute of Technology,

sponsored by the NASA/Army National Rotorcraft Technology Center, Ames Research Center, Moffett Field, California.

References

[1]Alexander, H. R., Smith, K. E., McVeigh, M. A., Dixon, P. G., and McManus, B. L., "Preliminary Design Study of Advanced Composite Blade and Hub and Nonmechanical Control System for the Tiltrotor Aircraft," NASA CR 152336-1, Nov. 1979.

[2]Lake, R. C., Nixon, M. W., Wilbur, M. L., Singleton, J. D., and Mirick, P. H., "Demonstration of an Elastically Coupled Twist Control Concept for Tilt Rotor Blade Application," *AIAA Journal*, Vol. 32, No. 7, 1994, pp. 1549–1551.

[3]Kosmatka, J. B., and Lake, R. C., "Extension-Twist Behavior of Initially Twisted Composite Spars for Tilt-Rotor Applications," *Proceedings of the 37th Structures, Structural Dynamics and Materials Conference*, Salt Lake City, Utah, Vol. 4, 1996, pp. 2175–2184.

[4]Moura, G. A., and Kolar, R., "Approach for Analysis and Design of Composite Rotor Blades," *Journal of Aircraft*, Vol. 29, No. 4, 1992, pp. 693–697.

[5]Chandra, R., and Chopra, I., "Structural Behavior of Two-Cell Composite Rotor Blades with Elastic Couplings," *AIAA Journal*, Vol. 30, No. 12, 1992, pp. 2914–2921.

[6]Barwey, D., and Peters, D. A., "Optimization of Composite Rotor Blades with Advanced Structural and Aerodynamic Modeling," *Mathematical Computer Modeling*, Vol. 19, No. 314, 1993, pp. 193–219.

[7]Ganguli, R., and Chopra, I., "Aeroelastic Optimization of a Helicopter Rotor with Composite Coupling," *Journal of Aircraft*, Vol. 32, No. 6, 1995, pp. 1326–1334.

[8]Chattopadhyay, A., McCarthy, T. R., and Seeley, C. E., "Decomposition-Based Optimization Procedure for High-Speed Prop-Rotors Using Composite Tailoring," *Journal of Aircraft*, Vol. 32, No. 5, 1995, pp. 1026–1033.

[9]Soykasap, Ö., and Hodges, D. H., "Aeroelastic Optimization of a Composite Tilt Rotor," AIAA Paper 98-1919, April 1998.

[10]Hodges, D. H., "A Mixed Variational Formulation Based on Exact Intrinsic Equations for Dynamics of Moving Beams," *International Journal of Solids and Structures*, Vol. 26, No. 11, 1990, pp. 1253–1273.

[11]Peters, D. A., and He, C.-J., "Correlation of Measured Induced Velocities with a Finite State Wake Model," *Journal of the American Helicopter Society*, Vol. 37, No. 3, 1991, pp. 55–70.

[12]Berdichevsky, V., Armanios, E., and Badir, A., "Theory of Anisotropic Thin-Walled Closed-Cross-Section Beams," *Composites Engineering*, Vol. 2, Nos. 5–7, 1992, pp. 411–432.

[13]Cesnik, C. E. S., Hodges, D. H., and Sutyrin, V. G., "Cross-Sectional Analysis of Composite Beams Including Large Initial Twist and Curvature Effects," *AIAA Journal*, Vol. 34, No. 9, 1996, pp. 1913–1920.

[14]Soykasap, Ö., "Aeroelastic Optimization of a Composite Tilt Rotor," Ph.D. Dissertation, School of Aerospace Engineering, Georgia Inst. of Technology, Atlanta, GA, Jan. 1999.

[15]Cesnik, C. E. S., and Hodges, D. H., "VABS: A New Concept for Composite Rotor Blade Cross-Sectional Modeling," *Journal of the American Helicopter Society*, Vol. 42, No. 1, 1997, pp. 27–38.

[16]Shang, X., "Aeroelastic Stability of Composite Hingeless Rotors with Finite-State Unsteady Aerodynamics," Ph.D. Dissertation, School of Aerospace Engineering, Georgia Inst. of Technology, Atlanta, GA, Aug. 1995.

[17]Arrington, W. L., Kumpel, M., Marr, R. L., and McEntire, K. G., "XV-15 Tilt Rotor Research Aircraft Flight Test Data Report, Vol. III: Structural Loads and Dynamics," NASA CR 177406, June 1985.

[18]Johnson, W., *Helicopter Theory*, Dover, New York, 1994, p. 263.

[19]Rand, O., Barkai, S. M., Carlson, R., and Peyran, R., "Modeling and Anaylsis of Tilt-Rotor Aeromechanical Phenomena," *Mathematical and Computer Modelling*, Vol. 27, No. 12, 1998, pp. 17–43.

[20]Vanderplaats, G. N., "ADS—A FORTRAN Program for Automated Design Synthesis, Version 1.10," NASA CR 177985, Sept. 1985.

[21]"NASA/ARMY XV-15 Tilt Rotor Research Aircraft," NASA TM X-62,407, Jan. 1975.

[22]Lentz, W. K., and Armanios, E. A., "Optimum Coupling in Thin-Walled, Closed-Section Composite Beams," *Journal of Aerospace Engineering*, Vol. 11, No. 3, 1998, pp. 81–89.

[23]Nixon, M. W., "Aeroelastic Response and Stability of Tiltrotors with Aeroelastically-Coupled Composite Rotor Blades," Ph.D. Dissertation, Dept. of Aerospace Engineering, Univ. of Maryland, College Park, MD, Dec. 1993.

[24]Popelka, D., Lindsay, D., Parham T., Berry, V., and Baker D. J., "Results of an Aeroelastic Tailoring Study for a Composite Tiltrotor Wing," *Journal of the American Helicopter Society*, Vol. 42, No. 2, 1997, pp. 126–136.